HHS Public Access

Author manuscript

J Biomed Mater Res B Appl Biomater. Author manuscript; available in PMC 2017 May 25.

Published in final edited form as:

J Biomed Mater Res B Appl Biomater. 2015 November ; 103(8): 1632–1640. doi:10.1002/jbm.b.33341.

In vitro biodegradation behavior, mechanical properties, and cytotoxicity of biodegradable Zn–Mg alloy

Haibo Gong[1], **Kun Wang**[2], **Randy Strich**[2], and **Jack G. Zhou**[1]

[1]Department of Mechanical Engineering and Mechanics, Drexel University, Philadelphia, Pennsylvania 19104

[2]Department of Molecular Biology, Rowan University, Stratford, New Jersey 08084

Abstract

Zinc–Magnesium (Zn–Mg) alloy as a novel biodegradable metal holds great potential in biodegradable implant applications as it is more corrosion resistant than Magnesium (Mg). However, the mechanical properties, biodegradation uniformity, and cytotoxicity of Zn–Mg alloy remained as concerns. In this study, hot extrusion process was applied to Zn–1 wt % Mg (Zn–1Mg) to refine its microstructure. Effects of hot extrusion on biodegradation behavior and mechanical properties of Zn–1Mg were investigated in comparison with Mg rare earth element alloy WE43. Metallurgical analysis revealed significant grain size reduction, and immersion test found that corrosion rates of WE43 and Zn–1Mg were reduced by 35% and 57%, respectively after extrusion. Moreover, hot extrusion resulted in a much more uniform biodegradation in extruded Zn–1Mg alloy and WE43. In vitro cytotoxicity test results indicated that Zn–1Mg alloy was biocompatible. Therefore, hot extruded Zn–1Mg with homogenous microstructure, uniform as well as slow degradation, improved mechanical properties, and good biocompatibility was believed to be an excellent candidate material for load-bearing biodegradable implant application.

Keywords

biodegradable metal; zinc alloy; extrusion; mechanical properties; cytotoxicity

INTRODUCTION

Biodegradable implants offer several advantages in load-bearing applications over their nondegradable counterparts used today. Prime among them is the promise that new implants based on these materials will eventually dissolve when they are no longer needed, hence eliminating residual implants or the pain and expense of a second removal surgery that could be required otherwise. These implants also facilitate tissue regeneration and healing by providing temporary mechanical support as diseased tissues restore their functions or new cells gradually replace the defects produced through biodegradation.[1–4] The amount of patients requiring surgical reconstruction is growing with the aging of the population, and the need of implanted devices for surgeries is huge. For example, for anterior cruciate

Correspondence to: J.G. Zhou, zhoug@drexel.edu.

ligament surgeries only, there are [mt]100,000 surgeries performed in the United States annually.[5]

It has been generally acknowledged that biodegradable metals are more suitable for load-bearing biodegradable implants due to their superior mechanical properties compared to polymeric materials.[6,7] Among several degradable metals, Magnesium (Mg) has attracted the most attention for its role in many important biological functions and its biocompatibility.[7] The main problem of magnesium is its rather rapid biodegradation, which occurs in the form of corrosion.[6,8] Rapid corrosion of Mg can compromise mechanical integrity during tissue recovery.[9,10] In addition, the rate at which some Mg alloys corrode may lead to rapid hydrogen evolution and alkalization of body fluids, both of which can overwhelm homeostatic mechanisms and further retard the healing process.[3,7,11]

Many new Mg alloys have been developed to solve the fast-corrosion problem, and among them WE43 was shown to be a suitable candidate Mg alloy for implant application, because it has sufficient mechanical properties and lower corrosion rate than most of other Mg alloys.[12] The first biodegradable Mg alloy stent, Lekton Magic coronary stent, was made out of WE43 by Biotronik. It was found that the 3-mm diameter stent had very high collapse pressure of 0.8 atm and low elastic recoil of 5%.[13] The major concern of Lekton Magic coronary stent was that it may lose its mechanical integrity in <4 weeks, while desired stent duration is at least 6 months.[13,14] WE43 was also used to make bone screws which demonstrated good biocompatibility and osteocondictivity.[15] No foreign body reactions, osteolysis, or systemic inflammatory reactions were detected.[15] However, the relatively rapid biodegradation of WE43 still remains as a concern.

Recent research showed that Zinc (Zn), as a more noble metal compared to Mg, can offer significant higher corrosion resistance without compromising mechanical integrity and biocompatibility.[16–18] Vojtěch et al.[17] investigated mechanical and in vitro biodegradation properties of as-cast Zn–Mg alloys with Mg ranging from 0.5 to 3 wt % (weight percentage). It was found that corrosion rate of Zn–Mg alloy was much lower than that of Mg alloy, and it did not change significantly with various Mg percentages. Their strength and elongation reached around 190 MPa and 1.8%, respectively, when adding Mg up to 1 wt %, but then dropped if adding Mg [mt]1 wt %, probably due to excessive amount of brittle eutectic phases. Bowen et al.[16] implanted pure Zn wire in rat abdominal aorta for up to 6 months and found that pure zinc remains intact for 4 months, after which time corrosion accelerates thus ensuring timely degradation of the implant.

The mechanical properties, biodegradation uniformity, and cytotoxicity of as-cast Zn–Mg alloy remained as concerns, although its corrosion resistance was considered as excellent for implant applications. For example, elongation of as-cast Zn–Mg alloy was about 1.8% at maximum when adding 1 wt % of Mg, but normally such low elongation would be considered as insufficient ductility for many biodegradable implant applications. Furthermore, Mg as a fast-corroding metal might cause nonuniform corrosion in Zn–Mg alloy, since as-cast Zn–Mg alloy has inherent nonuniform microstructure. Moreover, cytotoxicity of Zn–Mg alloy as a biodegradable metal must be examined against its possible adverse effects to cell growth. Unfortunately, up to now, there is no research paper published

to report methods of improving mechanical properties and biodegradation uniformity of Zn–Mg alloy and cytotoxicity of Zn–Mg alloy.

In this research, we sought to systematically investigate suitability of as-cast and extruded Zn–Mg alloys as biodegradable implant material in terms of mechanical properties, biodegradation uniformity, and cytotoxicity. Zn–1 wt % Mg (Zn–1Mg) alloy was selected due to its good mechanical properties as shown in previous study.[17] Mg alloy WE43, as a reference material, will be studied and compared with Zn–1Mg alloy. Biocompatibility of extruded Zn–1Mg will be evaluated through in vitro cell culture test.

MATERIALS AND METHODS

Sample preparation

To prepare Zn–1 wt % Mg (Zn–1Mg) alloy, pure Zn (99.99%) was melted in a resistance furnace and Mg chips (99.95%) were dipped in. A mechanical stir was used to homogenize the melt. A mixture of argon and SF_6 (1% volume ratio) was used as protection gas to prevent Mg from oxidation and achieve accurate alloy composition. The melt was casted in pure iron mould to make Zn–1Mg ingots, which were subsequently extruded at 200 °C and 20 mm/s with extrusion ratio of 16 to make cylindered rods. Commercially available WE43 ingots (Zibo Hongtai Anti-corrosion, China) were extruded at 400 °C at 20 mm/s with extrusion ratio of 16 to make cylindered rods. Chemical compositions of Zn–1Mg and WE43 were analyzed through inductively coupled plasma atomic emission spectrometry.

Metallurgical analysis

Specimens were ground by silicon carbide abrasive papers with successive grades from 400 to 2000 and polished with 0.5 μm diamond suspension. Polished specimen were etched by picric solution (10 mL acetic acid, 4.2 g picric acid, 10 mL H_2O, and 70 mL ethanol) and examined with scanning electron microscope (SEM, Philips XL-30, USA) equipped with energy-dispersive X-ray spectroscopy (EDX) and backscattered electron (BSE) detectors. To reveal microstructures of certain alloy, SEM images were taken at specific magnification chosen to suit each alloy's grain size level.

Immersion test in SBF

Specimens (diameter 10 mm × thickness 3 mm) were cut from extruded Zn–1Mg and WE43 rods, ground up to 2000 grit, and washed using acetone, ethanol, and deionized water (ASTM type II) in ultrasonicator in sequence.

In vitro biodegradation behaviors of Zn–Mg and WE43 alloy were evaluated through immersion test according to ASTM-G31-72[19] in simulated body fluid (SBF).[20] Briefly, SBF (Table I) were added into the testing containers by the surface area to solution volume at 1 cm^2:100 mL and refreshed every 24 h. The temperature was kept at 37 °C. Samples were removed after 7 days, gently rinsed with deionized water, and dried at room temperature. Corrosion products were evaluated using SEM with an EDX. After that, corrosion products were removed by washing in distilled water first and then in chromic acid solution (200 g/L Cr_2O_3) for 5 min at 40 °C in ultrasonicator, and corrosion morphology was observed using

SEM. For Mg alloy, chromic acid solution contained 10 g/L $AgNO_3$. Dry weights of samples before corrosion test and after removing corrosion products were measured to calculate corrosion rate using following formula:

$$\text{Corrosion rate} = (K \times W)/(A \times T \times D) \quad (1)$$

where K is a constant (8.76×10^4 for rate unit of millimeter per year), W is mass loss in gram, A is area in cm^2, T is time of exposure in hours, and D is density in g/cm^3.

Tensile test

Tensile test samples were machined according to ASTM-E8-04.[21] The tensile tests were performed on a MTS single axis servohydraulic testing system at a displacement rate of 0.5 mm/min. Fracture morphology was observed using SEM.

Biocompatibility test

Indirect cytotoxicity test was performed according to ISO 10993-52009.[22] To prepare extract mediums, metal samples were cleaned, sterilized, and incubated in Dulbecco's modified Eagle's medium with 10% fetal bovine serum for 72 h under physiological conditions (5% CO_2, 20% O_2, 95% humidity, 37 °C). The supernatant fluid is withdrawn and filtered by 0.2 μm filter. Fibroblast (L-929) cells were seeded in 96-well plate at 5000 cells per well density for overnight. The medium was replaced with 100 μl per well metal extract (1:15 dilution) in the next day. After further incubation for either 24 h or 72 h, 10 μL 3-(4,5-Dimethylthiazol-2-yl)-2,5-Diphenyltetrazolium Bromide (MTT) solution (5 mg/ml, from Sigma-Aldrich) was added to each well. The plate was then incubated for another 4 h at 37 °C. Then, the medium was carefully removed and 100 μL MTT solvent solution (1:1 Dimethyl sulfoxide (DMSO) and isopropanol) was added to each well. The plate was incubated for 15 min at room temperature and then absorbance was read at 570 nm. Extract medium without cells was used as control for absorbance reading.

For cell adhesion test, Zn–1Mg and WE43 samples were cleaned by ethanol, air-dried, and UV sterilized overnight, and then put into a 24-well plate. L-929 cells were seeded on the samples at a density of 1×10^5 cells per mL. Cell culture medium was changed at the next day. After 48 h, cells were stained with 5 μg/mL Hochest 33342 (Molecular Probes) for 30 min. Then the samples were fixed with 4% paraformaldehyde for 15 min at room temperature and then permeabilized by 0.1% Triton X-100 for 20 min at 4°C. After that, cells were stained with 50 μg/mL rhodamine phalloidin (Sigma-Aldrich) for 30 min at room temperature. Samples were visualized under Nikon confocal microscope.

Statistics

Three samples were tested at each time point for the immersion test and cell viability test. Student's t test was performed to evaluate the significance of difference. Two groups of results with p value less than 0.05 was considered as significant different.

RESULTS

Microstructure analysis

Elemental compositions of as-cast WE43 and Zn–1Mg was shown in Table II. As shown in Figure 1(a,b), microstructure of as-cast WE43 consisted of α-Mg matrix and precipitates (arrow). The size of α-Mg grain is about 50–80 μm, while polyhedral and sphere precipitates are around several microns and sub-micron in size, respectively. SEM/EDX analysis showed that the precipitates along grain boundary contained 10.93 wt % (weight percentage) of Yttrium (Y) and 17.12 wt % of Nd and was named as Mg (RE,Y). Typical polyhedral precipitates contained more than 82.22 wt % of Y and Zr was found in sphere precipitates (Table III). These results are consistent with results from Coy et al.[23]

Figure 1(c,d) showed that grain size of extruded WE43 was about 5 μm, which was much smaller than that of as-cast WE43. Another obvious characteristic of grain refinement after extrusion is that grain structure changed from dendritic grains to near-hexagon equiaxed grains. Precipitates were randomly observed segregated along grain boundary and within α-Mg grain.

Coarse microstructure of as-cast Zn–1Mg consisted of primary Zn dendritic grains and eutectic phase in between primary grains [Figure 2(a,b)]. The size of most Zn dendritic grains is about 50–100 μm while smaller grains, for example, 10 μm, were also observed. SEM/EDX analysis revealed that a primary Zn grain is mainly composed of Zn, while eutectic phase is a mixture of Zn and Mg (Table IV). Solubility of Mg in Zn is less than 0.01 wt % thus Mg was not detected in Zn grains by SEM/EDX due to limited measuring resolution.

Similar to WE43, grain refinement of Zn–Mg was also observed after extrusion, as large dendritic Zn grains evolved into small near-equiaxed grains [Figure 2(c,d)]. Moreover, eutectic mixture disappeared and instead precipitates segregated along grain boundaries. It was found that composition of precipitates was 94.99 Zn–5.01 Mg (at %).

With only 1 wt % of Mg, Zn–Mg alloy was already found with high volume ratio of eutectic phase at grain boundary, because solid solubility of Mg in Zn is lower than 0.01 wt %. During deformation process, recrystallization occurred and as a result, large dendritic grains of as-cast Zn–1Mg disappeared and uniform small equiaxial grains formed [Figure 2(c)]. In the same time, eutectic phase transformed into smaller precipitates due to high temperature and high shear stress generated during deforming process.

In vitro corrosion rates and biodegradation products in SBF

As shown in Table V, in vitro corrosion rate of WE43 in SBF was reduced by 35% after extrusion. During biodegradation process, large amount of salt precipitation was attracted on sample surface and it formed a layer covering the surface (Figure 3). SEM/EDX analysis showed that Ca^{2+}, carbonate, and phosphate ions in SBF reacted with Mg, Yttrium (Y), and rare earth (RE) elements during the biodegradation process (Figure 4).[24]

Compared with WE43, Zn–1Mg was much more corrosion-resistant, and corrosion rate of Zn–1Mg in SBF is much lower. This finding is consistent with previous research by Vojtěch et al.[17] Moreover, corrosion rate reduction of Zn–1Mg in SBF after extrusion was much more significant, that is, 57% (Table V). Top layer of biodegradation products of Zn–1Mg were mainly composed of Zn, O, P, and Ca (Figures 5 and 6). It is reasonable to assume that they may contain ZnO, $Zn(OH)_2$, $Zn_3(PO_4)_2$, and $Ca_3(PO_4)_2$. This is probably because of the ionic interaction between Zn biodegradation products and chloride, hydrogen phosphate and hydrogen carbonate in SBF.

In vitro biodegradation uniformity in SBF

Figure 7(a,c) shows that biodegradation morphology of as-cast WE43 and Zn–1Mg is generally nonuniform, showing obvious microgalvanic corrosion between metal matrix and precipitates segregated along grain boundary. The large intermetallic compounds in as-cast WE43 and wide eutectic mixtures in as-cast Zn–1Mg may be the primary cause of the severe microgalvanic corrosion, respectively. In contrast, biodegradation morphology of extruded WE43 and Zn–1Mg at similar magnification was generally uniform without extensive microgalvanic corrosion [Figure 7(b,d)].

Tensile property and fracture morphology

Strength and elongation of WE43 were simultaneously improved after extrusion process, probably due to grain refinement and enhanced grain boundary strengthening effect (Figure 8). Increase of yield strength and elongation are 1.6 and 5 times, respectively.

In a similar way, strength and elongation of Zn–1Mg was significantly increased after extrusion process, but increase of elongation after extrusion is much higher compared to WE43, that is, 10 versus 5 times. It seems that after similar extrusion process the change of mechanical properties of as-cast Zn alloy is more significant compared with that of as-cast Mg alloy. For example, elongation of pure Zn reached 54% after extrusion, while extruded pure Mg only has elongation of around 8%.[25,26]

Compared to that of extruded pure Zn, strength of extruded Zn–1Mg was nearly twice higher, but elongation of extruded Zn–1Mg was much lower. It seemed that Mg was an effective strengthening alloying element for Zn, but decrease of ductility after adding Mg must be considered when designing Zn–Mg alloy formula.

By comparing mechanical properties of extruded pure Zn and Zn–1Mg, it can be hypothesized that the precipitates surrounding primary Zn grains can not only provide resistance to crack propagation during failure, resulting strengthening effect but can also initiate microcracking under stress and cause reduction in elongation.

Extruded pure Zn exhibited typical dimple fracture features, and this is consistent with its excellent elongation performance [Figure 9(a)]. The fracture morphology of extruded Zn–1Mg was quasi-cleavage fracture, a mixture of brittle and ductile fracture [Figure 9(b)].

Biocompatibility test

To evaluate cytotoxicity of Zn–1Mg, metabolic activity of fibroblast cells (L-929) were measured through MTT test after cell culture for 24 and 72 h. Cells were cultured in different mediums, including regular medium as control and extraction medium of Zn–1Mg, for 24 and 72 h. Viability percentages versus control group were demonstrated in Figure 10.

Compared with that of control group, cell viability at 24 h was not significantly affected by extract medium of Zn–1Mg (Figure 10). Similar patterns were found in cell culture results at 72 h. Cells showed good tolerance to Zn–1Mg extract medium and cell morphologies in all groups were normal and healthy (Figure 11). This indicates degradation products of Zn–1Mg did not have significant impact on cell growth and metabolic activity, thus Zn–1Mg could be considered as nontoxic and biocompatible materials.

Cell adhesion experiment was performed to evaluate cell attachment ability of L-929 on WE43 and Zn–1Mg. Figure 12 shows fluorescence-stained L-929 successfully adhered on both WE43 and Zn–1Mg. These results were consistent with cell viability test and indicate Zn–1 g can support cell attachment and growth.

DISCUSSION

The main advantage of Zn–Mg alloy over Mg alloy is its high corrosion resistance in body fluid environment, considering current Mg alloy implants often suffer from fast-corrosion and consequent release of hydrogen bubble and early dislocation and disruption. In addition, Hennig et al.[27] found that zinc as antioxidant and endothelial membrane stabilizer exhibited strong antiatherogenic properties, enhanced endothelium integrity and protected constituent cells from lipid-or cytokine-induced perturbation. Moreover, Yamaguchi et al.[28] found that the presence of zinc has produced appreciable increases in several parameters of bone mineralization such as bone calcium content, alkaline phosphatase activity, and collagen content in rat calvarias tissue culture. Therefore, from biological aspect, released zinc from Zn–Mg alloy implants degradation may exemplify many of the advantages gained by using biodegradable orthopedic implants and coronary stents.

Uniform biodegradation through homogeneous corrosion is critical to success of load-bearing biodegradable implant. Nonuniform biodegradation of load-bearing implant may be catastrophic, because inhomogeneous mass loss leads to localized stress concentration and unexpected early disrup-ture.[29,30] This is even more important to Zn–Mg alloy since it is more susceptible to micro-galvanic corrosion, due to larger potential difference between Zn matrix and precipitates.

As shown in Figure 7, nonuniform biodegradation seemed to be more significant for as-cast Zn–1Mg in comparison with as-cast WE43 and cracks at boundary after corrosion were deeper. Well controlled casting and thermal deformation process is necessary to achieve homogenous microstructure and uniform biodegradation of biodegradable metals. In this research, hot extrusion was shown to be beneficial to hinder nonuniform microgalvanic corrosion of Zn alloy. First of all, hot extrusion process resulted in a general homogenization of chemical distribution by grain refinement and heat treatment. Large precipitates were

breaking down and uniformly spread throughout the metal matrix. Moreover, galvanic corrosion current at each microgalvanic corrosion site would drop because cathode surface decreased significantly due to size reduction of precipitates (cathode) during hot extrusion process.[31] These will consequently result in a relatively uniform corrosion and biodegradation in extruded WE43 and Zn–Mg alloy.

As shown in Figure 8, Mg alloying exhibited effective strengthening effect for Zn alloy, but decrease of ductility after adding Mg must be considered when designing Zn–Mg alloy formula, since 10% of elongation may be too low for applications such as coronary stent. According to Zn–Mg phase diagram, solid solubility of Mg in Zinc is lower than 0.01 wt %, and precipitates form even at small amount addition of Mg, as shown in Figure 2. Eutectic point corresponds to about 3 wt % of Mg, thus Mg concentration must be lower than 3 wt %, otherwise Zn–Mg alloy will mainly contain brittle eutectic phase.[17] It is thus proposed that optimal Mg concentration falls in between 0.01 wt % and 3 wt %. In future study, alloy formula will be adjusted by optimizing mechanical properties and biodegradation behaviors.

In vitro cytotoxicity test results indicated that Zn–1Mg alloy was not toxic, since cells growing in contact with corrosion products of Zn–1Mg maintained high cell viability and healthy morphology. Zn–1Mg was shown to support cell adhesion and L-929 cells successfully attached on Zn–1Mg after 24 h of cell culture. However in future study, animal study will be necessary to characterize Zn–Mg in terms of in vivo toxicity including both toxicity to local tissue and systematic toxicity to various organs.[32,33] Local accumulation of Zn ions in certain physiological environment need to be further accessed.

CONCLUSION

Corrosion rate of as-cast Zn–1Mg was found to be much lower than that of WE43, but as-cast Zn–1Mg suffered from significant nonuniform microgalvanic corrosion. After hot extrusion both biodegradation uniformity and mechanical properties of WE43 and Zn–1Mg were improved. Typical grain refinement effect in Zn–1Mg after hot extrusion was characterized by the transformation of large dendritic grains into small near-equiaxed grains, and the change of wide eutectic mixture into small intermetallic precipitates segregated along grain boundaries. More importantly, hot extrusion resulted in a much more uniform biodegradation in extruded WE43 and Zn–1Mg alloy. In addition, strength and elongation of WE43 and Zn–1Mg were simultaneously improved after extrusion process, probably due to grain refinement during extrusion process. In vitro cytotoxicity test results indicated that Zn–1Mg alloy was biocompatible, as cells growing in contact with corrosion products of Zn–1Mg maintained high cell viability and healthy morphology. It's thus believed that extruded Zn–1Mg alloy with homogenous microstructure, uniform and slow biodegradation, improved mechanical properties and good biocompatibility is a suitable candidate material for load-bearing biodegradable implant application.

Acknowledgments

We gratefully thank the Centralized Research Facility (CRF) of the College of Engineering, Drexel University for providing access to electronic microscopes used in this work. We also thank Prof. Vojtěch for his help in Zn alloy

casting process, Juan Wang for her help in Mg corrosion study, and Kavan Hazeli and Prof. Antonios Kontsos for their help in metallurgical analysis of Mg alloy.

References

1. Hermawan, H. Biodegradable Metals. Berlin Heidelberg: Springer; 2012. Biodegradable Metals: State of the Art; p. 13-22.
2. Yun Y, Dong Z, Lee N, Liu Y, Xue D, Guo X, Kuhlmann J. Revolutionizing biodegradable metals. Mater Today. 2009; 12:22–32. DOI: 10.1016/S1369-7021(09)70273-1
3. Moravej M, Mantovani D. Biodegradable metals for cardiovascular stent application: Interests and new opportunities. Int J Mol Sci. 2011; 12:4250–4270. [PubMed: 21845076]
4. Gong H, Agustin J, Wootton D, Zhou J. Biomimetic design and fabrication of porous chitosan–gelatin liver scaffolds with hierarchical channel network. J Mater Sci: Mater Med. 2014; 25:113–120. [PubMed: 24121873]
5. Suomalainen P, Moisala A-S, Paakkala A, Kannus P, Järvelä T. Comparison of tunnel placements and clinical results of single-bundle anterior cruciate ligament reconstruction before and after starting the use of double-bundle technique. Knee Surg Sports Traumatol Arthrosc. 2013; 21:646–653. [PubMed: 22527410]
6. Staiger MP, Pietak AM, Huadmai J, Dias G. Magnesium and its alloys as orthopedic biomaterials: A review. Biomaterials. 2006; 27:1728–1734. [PubMed: 16246414]
7. Witte F, Hort N, Vogt C, Cohen S, Kainer KU, Willumeit R, Feyerabend F. Degradable biomaterials based on magnesium corrosion. Curr Opin Solid State Mater Sci. 2008; 12:63–72.
8. Seal, C., Vince, K., Hodgson, M. Biodegradable surgical implants based on magnesium alloys–A review of current research. IOP Conference Series: Materials Science and Engineering; Philadelphia, PA: IOP Publishing; 2009.
9. Zeng R, Dietzel W, Witte F, Hort N, Blawert C. Progress and challenge for magnesium alloys as biomaterials. Adv Eng Mater. 2008; 10:B3–B14.
10. Krause A, von der Höh N, Bormann D, Krause C, Bach F-W, Windhagen H, Lindenberg AM. Degradation behaviour and mechanical properties of magnesium implants in rabbit tibiae. J Mater Sci. 2010; 45:624–632.
11. Erinc, M., Silekens, WS., Mannens, R. Magnesium Technology. San Francisco, CA, USA: 2009. Applicability of existing magnesium alloys as biomedical implant materials; p. 209-214.
12. Gu XN, Zhou WR, Zheng YF, Cheng Y, Wei SC, Zhong SP, Xi TF, Chen LJ. Corrosion fatigue behaviors of two biomedical Mg alloys—AZ91D and WE43—in simulated body fluid. Acta Biomater. 2010; 6:4605–4613. [PubMed: 20656074]
13. Onuma Y, Ormiston J, Serruys PW. Bioresorbable scaffold technologies. Circ J. 2011; 75:509–520. [PubMed: 21301138]
14. Di Mario C, Griffiths HUW, Goktekin O, Peeters N, Verbist JAN, Bosiers M, Deloose K. Drug-eluting bioabsorbable magnesium stent. J Interv Cardiol. 2004; 17:391–395. [PubMed: 15546291]
15. Windhagen H, Radtke K, Weizbauer A, Diekmann J, Noll Y, Kreimeyer U, Schavan R, Colsman CS, Waizy H. Biodegradable magnesium-based screw clinically equivalent to titanium screw in hallux valgus surgery: Short term results of the first prospective, randomized, controlled clinical pilot study. Biomed Eng Online. 2013; 12:62. [PubMed: 23819489]
16. Bowen PK, Drelich J, Goldman J. Zinc exhibits ideal physiological corrosion behavior for bioabsorbable stents. Adv Mater. 2013; 25:2577–2582. [PubMed: 23495090]
17. Vojtěch D, Kubásek J, Šerák J, Novák P. Mechanical and corrosion properties of newly developed biodegradable Zn-based alloys for bone fixation. Acta Biomater. 2011; 7:3515–3522. [PubMed: 21621017]
18. Dambatta M, Izman S, Hermawan H, Kurniawan D. Influence of heat treatment cooling mediums on the degradation property of biodegradable Zn–3Mg Alloy. Adv Mater Res. 2014; 845:7–11.
19. Standard, A. Annual Book of ASTM Standards. West Conshohocken, USA: ASTM International; 2004. G31-72. Standard Practice for Laboratory Immersion Corrosion Testing of Metals" (Reapproved 1990); p. 302

20. Kokubo T, Kushitani H, Sakka S, Kitsugi T, Yamamuro T. Solutions able to reproduce in vivo surface-structure changes in bioactive glass-ceramic A-W3. J Biomed Mater Res. 1990; 24:721–734. [PubMed: 2361964]
21. Standard, A. Annual Book of ASTM Standards. West Conshohocken, USA: ASTM International; 2004. E8-04. Standard Test Methods for Tension Testing of Metallic Materials; p. 3
22. Standard, I. Biological Evaluation of Medical Devices—Part 5: Tests for In Vitro Cytotoxicity. Geneve, Switzerland: International Organization for Standardization; 2009.
23. Coy AE, Viejo F, Skeldon P, Thompson GE. Susceptibility of rare-earth-magnesium alloys to micro-galvanic corrosion. Corros Sci. 2010; 52:3896–3906.
24. Zhang S, Li J, Song Y, Zhao C, Zhang X, Xie C, Zhang Y. In vitro degradation, hemolysis and MC3T3-E1 cell adhesion of biodegradable Mg–Zn alloy. Mater Sci Eng C. 2009; 29:1907–1912.
25. Stanford N, Barnett MR. The origin of "rare earth" texture development in extruded Mg-based alloys and its effect on tensile ductility. Mater Sci Eng A. 2008; 496:399–408.
26. Haibo Gong, AK., Kim, Y., Lelkes, PI., Zhang, Q., Yao, D., Hazeli, K., Zhou, JG. Micro characterization of Mg and Mg alloy for biodegradable orthopedic implants application. ASME International Manufacturing Science and Engineering Conference; 2012; Notre Dame, IN, USA. p. 891-895.
27. Hennig B, Toborek M, McClain CJ. Antiatherogenic properties of zinc: Implications in endothelial cell metabolism. Nutrition. 1996; 12:711–717. [PubMed: 8936496]
28. Yamaguchi M, Oishi H, Suketa Y. Stimulatory effect of zinc on bone formation in tissue culture. Biochem Pharmacol. 1987; 36:4007–4012. [PubMed: 3689432]
29. Mao L, Shen L, Niu J, Zhang J, Ding W, Wu Y, Fan R, Yuan GY. Nanophasic biodegradation enhances the durability and biocompatibility of magnesium alloys for the next-generation vascular stents. Nanoscale. 2013; 5:9517–9522. [PubMed: 23989064]
30. Ghali E, Dietzel W, Kainer K-U. General and localized corrosion of magnesium alloys: A critical review. J Mater Eng Perform. 2004; 13:7–23.
31. Arya C, Vassie PRW. Influence of cathode-to-anode area ratio and separation distance on galvanic corrosion currents of steel in concrete containing chlorides. Cem Concr Res. 1995; 25:989–998.
32. Bowen PK, Drelich J, Goldman J. A new in vitro–in vivo correlation for bioabsorbable magnesium stents from mechanical behavior. Mater Sci Eng C. 2013; 33:5064–5070.
33. Bowen PK, Drelich A, Drelich J, Goldman J. Rates of in vivo (arterial) and in vitro biocorrosion for pure magnesium. J Biomed Mater Res A. 2014

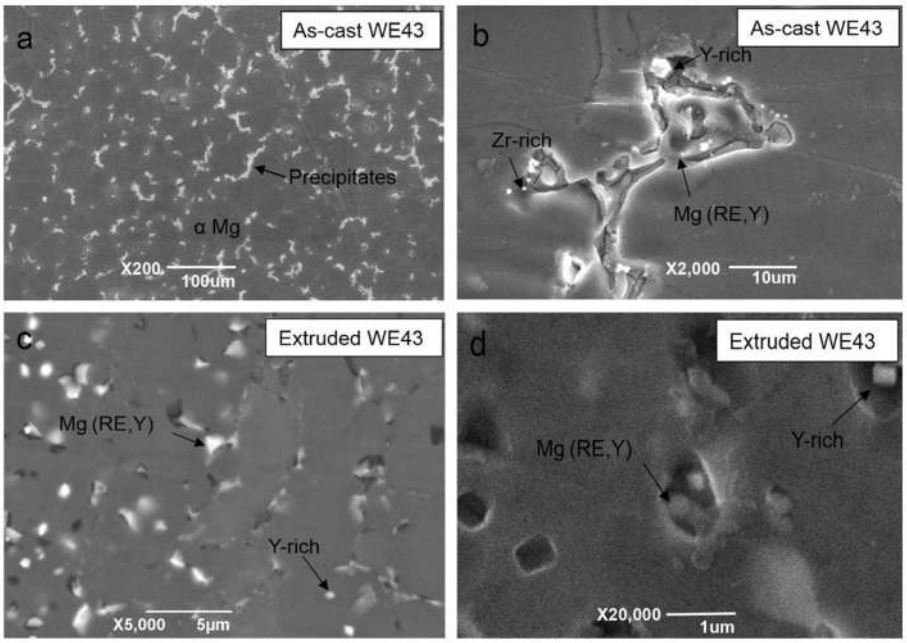

FIGURE 1.

Metallurgical analysis of as-cast (a, b) and extruded (c, d) WE43. Arrow shows intermetallic compounds and precipitates.

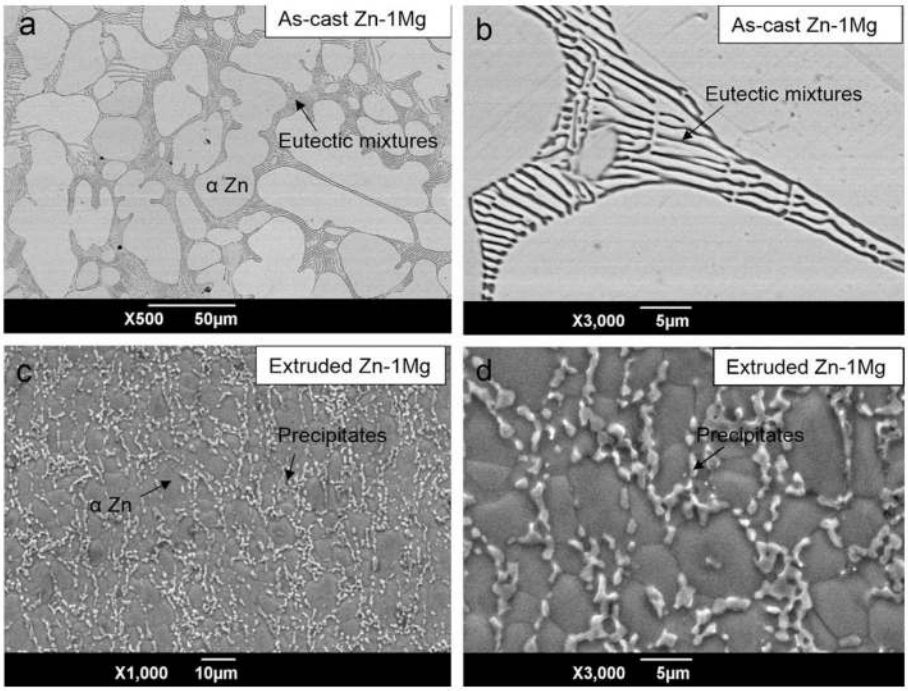

FIGURE 2.

Grain structure of as-cast (a, b) and extruded (c, d) Zn–1Mg. Arrow in b shows eutectic mixtures and arrow in d shows intermetallic precipitates.

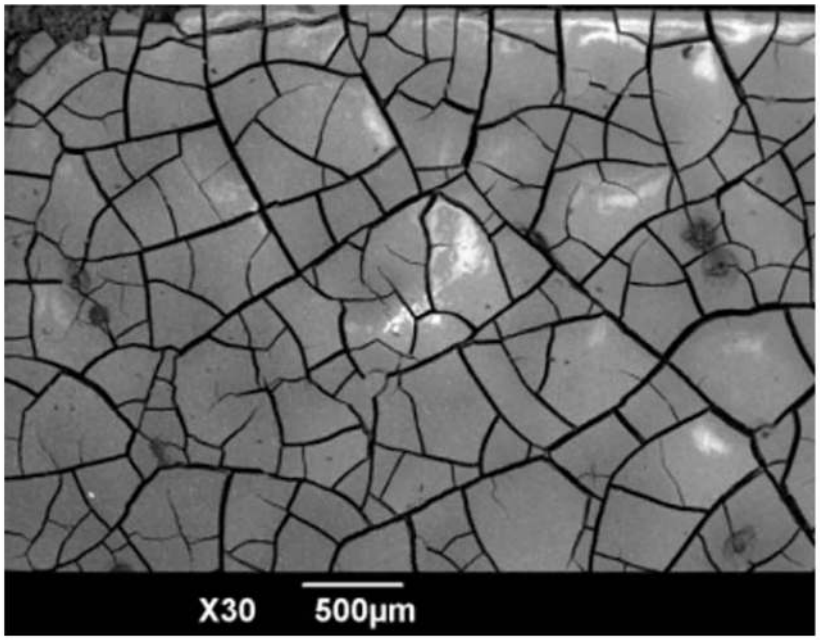

FIGURE 3.
Morphology of corrosion products of WE43 in SBF before acid washing.

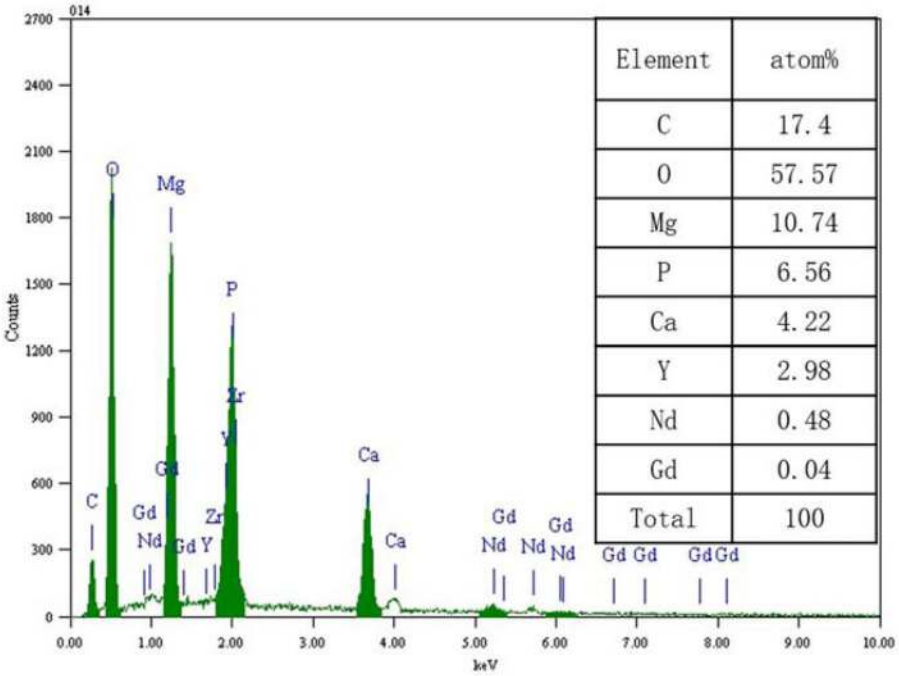

FIGURE 4.

Elemental composition of corrosion products of WE43 in SBF. [Color figure can be viewed in the online issue, which is available at wileyonlinelibrary.com.]

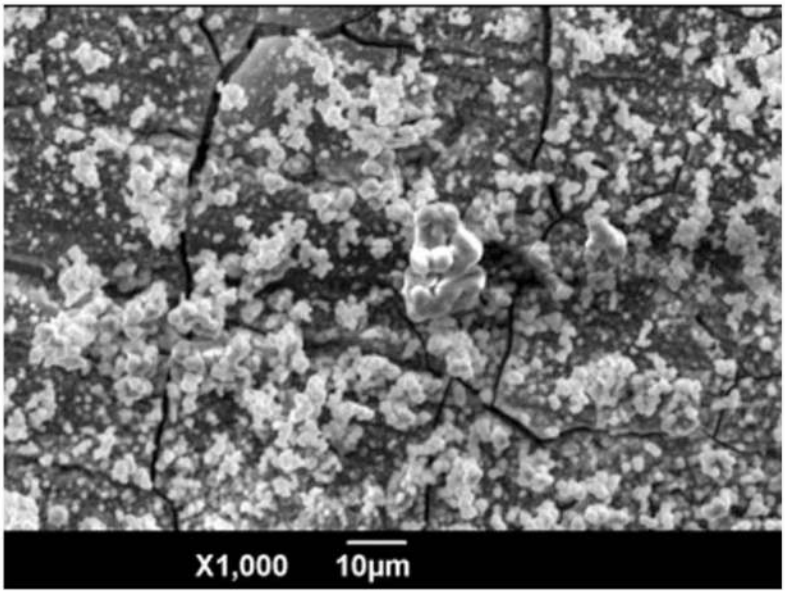

FIGURE 5.
Morphology of corrosion products of Zn–1Mg in SBF before acid washing.

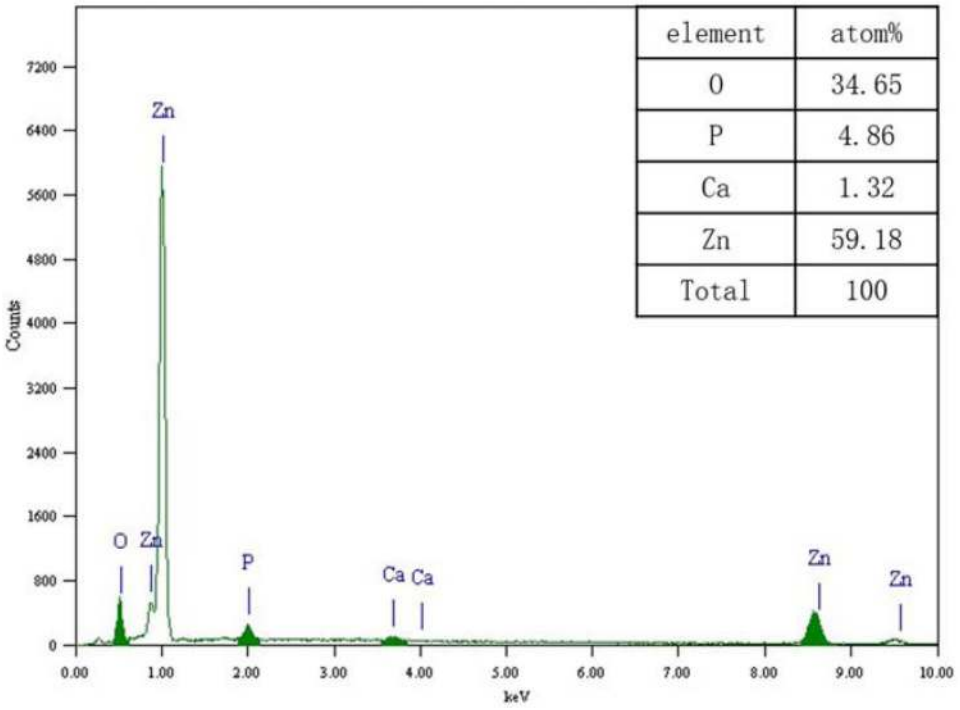

FIGURE 6.

Elemental composition of corrosion products of Zn–1Mg in SBF. [Color figure can be viewed in the online issue, which is available at wileyonlinelibrary.com.]

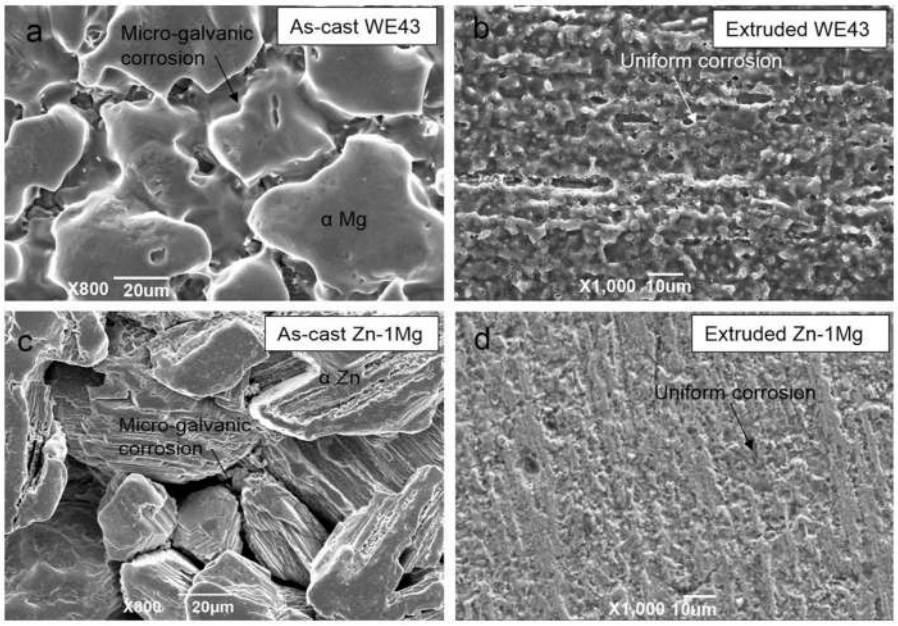

FIGURE 7.

Corrosion morphology of WE43 (a, b) and Zn–1Mg (c, d) in SBF after acid washing. Arrow shows intergranular corrosion.

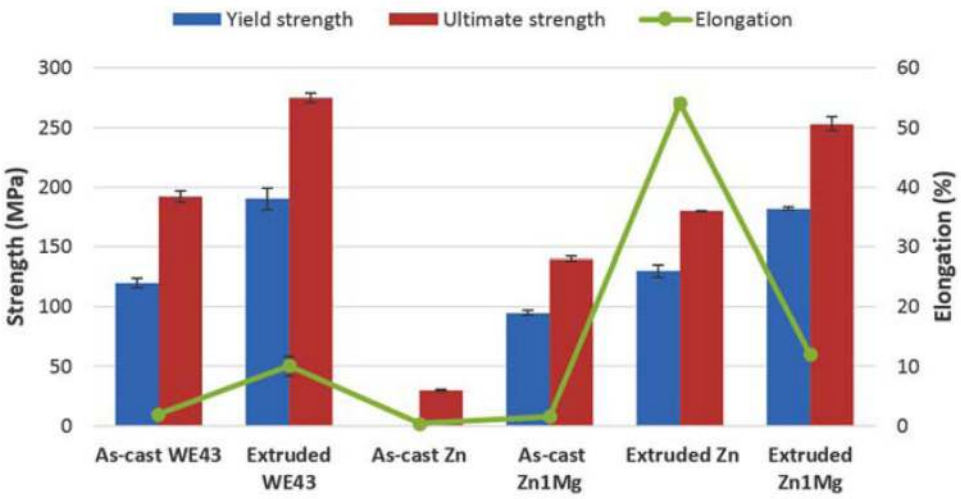

FIGURE 8.

Tensile properties of as-cast and extruded WE43, pure Zn and Zn–1Mg. Only ultimate strength was available because as-cast Zn specimen cracked before plastic deformation. [Color figure can be viewed in the online issue, which is available at wileyonlinelibrary.com.]

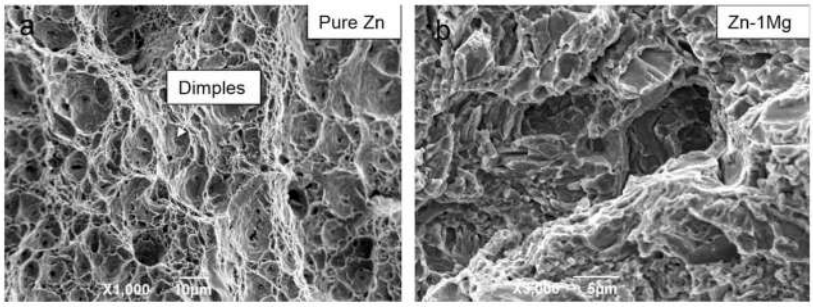

FIGURE 9.
Fracture morphology of extruded pure Zn and Zn–1Mg after tensile test.

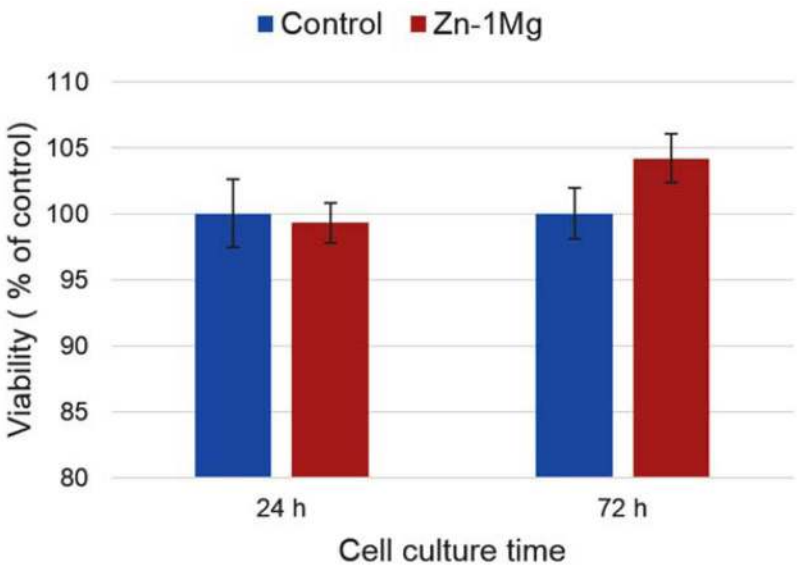

FIGURE 10.

Cell viability of fibroblast cells (L-929) cultured in regular media (control) and extraction media of extruded Zn–1Mg. [Color figure can be viewed in the online issue, which is available at wileyonlinelibrary.com.]

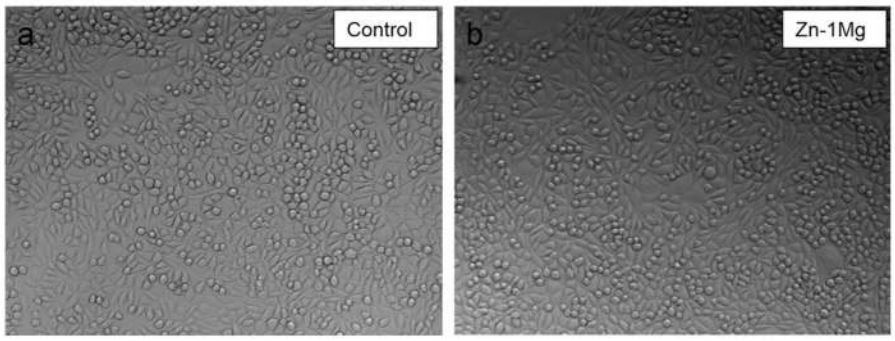

FIGURE 11.

Optical images of fibroblast (L-929) cells after 72 h of culture in regular media (a, control) and extraction media of extruded Zn–1Mg (b).

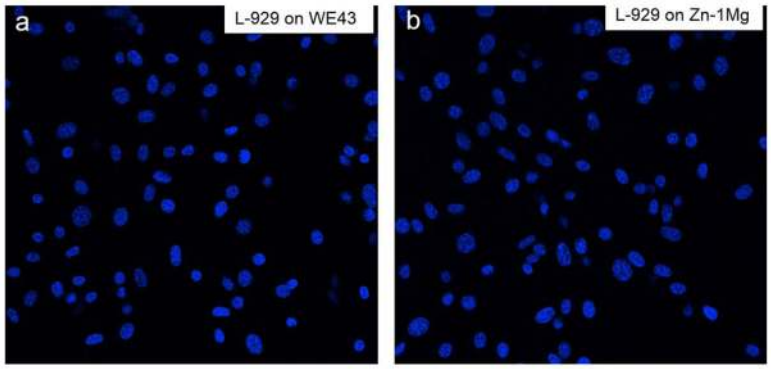

FIGURE 12.
Fluorescent images of fibroblast (L-929) cells growing on WE43 and Zn–1Mg for 24 h.

TABLE I

Reagents for Preparing SBF (pH 7.40, 1 L)

Order	Reagent	Amount
1	NaCl	7.996 g
2	$NaHCO_3$	0.350 g
3	KCl	0.224 g
4	K_2HPO_4	0.174 g
5	$MgCl_2{\cdot}6H_2O$	0.305 g
6	1*M* HCl	30 mL
7	$CaCl_2{\cdot}2H_2O$	0.368 g
8	Na_2SO_4	0.071 g
9	$(CH_2OH)_3CNH_2$	6.057 g

TABLE II

Elemental Composition of As-Cast WE43 and Zn–1Mg Alloy

	Element (Weight %)							
Alloy	**Mg**	**Zn**	**Y**	**Nd[a]**	**Gd[a]**	**Zr**	**Fe**	**Al**
WE43	92.69	N	3.94	2.73	0.27	0.36	<0.01	<0.01
Zn–1Mg	0.95	99.04	N	N	N	N	<0.01	<0.01

[a]Yttrium (Y), Neodymium (Nd).

J Biomed Mater Res B Appl Biomater. Author manuscript; available in PMC 2017 May 25.

TABLE III

Elemental Composition of Microconstitutes in As-Cast and Extruded WE43

		Weight %				
Alloy	**Microconstitute**	**Mg**	**Y**	**Nd**	**Gd**	**Zr**
As-cast WE43	α-Mg	92.44	6.65	0.91		
	Mg (RE, Y)	71.95	10.93	17.12		
	Y-rich	5.30	82.22	6.05	6.42	
	Zr-rich	53.15	34.96	4.89	4.74	2.26
Extruded WE43	α-Mg	90.10	7.79	2.11		
	Mg (RE, Y)	68.79	12.82	18.39		
	Y-rich	53.17	36.62	4.07	6.13	
	Zr-rich	80.38	11.95	6.22		1.45

J Biomed Mater Res B Appl Biomater. Author manuscript; available in PMC 2017 May 25.

TABLE IV

Elemental Composition of Microconstitute in As-Cast and Extruded Zn–1Mg

		Weight %	
Alloy	**Microconstitute**	**Zn**	**Mg**
As-cast Zn–Mg	α phase	100	0
	Eutectic phase	97.03	2.97
Extruded Zn–Mg	α phase	100	0
	Precipitates	94.99	5.01

TABLE V

Corrosion Rate of As-Cast and Extruded WE43 and Zn–1Mg

	As-cast WE43	Extruded WE43	As-cast Zn–1Mg	Extruded Zn–1Mg
Corrosion rate (mm/year)	6.64 ± 0.06	4.34 ± 0.02	0.28 ± 0.01	0.12 ± 0.05